

# Chapter Two

## *Specimen interaction and information generated with electron beam instruments.*

### 2. Specimen interaction

Electron beam instruments are so versatile in part because of the number of different types of interactions which take place between primary-beam electrons and atoms within the specimen. When primary electrons collide with atoms within the specimen they impart energy to the specimen. Any "event" resulting in a loss of energy (or change in momentum) of the primary-beam electrons (hereafter referred to simply as primary electrons) must produce an equivalent amount of energy in some other form. There are numerous forms of energy phenomena produced during electron - specimen interaction, and all of these have the potential to provide important information about the nature of the specimen.

Whenever a primary electron penetrates a sample being bombarded, it interacts with the atoms within the specimen. Each interaction "event" results in a loss of energy (or change in momentum) of a primary electron, and ultimately the electron's energy is diminished and/or direction of flight is modified. The 3-dimensional space in which primary-beam electrons have sufficient energy to interact with the specimen is known as *the interaction volume*. As an electron travels through the interaction volume, it is said to *scatter*; that is, lose energy and change direction with each atomic interaction. *Scattering events* can be divided into two general classes: **1. elastic scattering**, in which the electron exchanges little or no energy, but changes direction; and **2. inelastic scattering**, in which the electron exchanges significant, and definite, amounts energy, but has its direction virtually unchanged. Both types of events determine the size and shape of the interaction volume. Inelastic scattering events are responsible for the wide variety of *characteristic* (i.e., element specific) and non-specific information, which can be emitted and detected from the specimen. These include secondary electrons, Auger electrons, characteristic and continuum x-rays, long-wavelength radiation in the visible, IR and UV spectral range (cathodoluminescence), lattice vibrations or phonons, and electron oscillations or plasmons. The inelastic scattering events, because many of them are element specific, are especially useful in quantitative EPMA. For our purposes, the elastic scattering events are important in that they (1) produce backscattered electrons and (2) change the shape of the scattering volume (that is the depth to lateral scattering spatial ratio).

The primary beam of electrons is focused onto a spot on the specimen surface, the diameter of which can be as small as 5nm. *Spot size* is what sells electron microscopes because

it determines the degree with which we can *magnify*<sup>1</sup> and still discern detail from one point to the next (the distance between discernible points is defined as *resolution*, and is sometimes equated with the spot size). It is important to understand the relationship between spot size and interaction volume. If the energy form we are measuring is generated within the specimen from scattering events, it is likely to have come from an area at the surface considerably larger than the spot size (that is, imagine the area from which information is emitted through the surface being much larger than the entry area). If, for example, a particular form of energy is generated at  $1\mu$  depth, then the resolution for that kind of information will have a similar horizontal dimension, approximately  $1\mu$ , or 200 times the spot size of  $5\text{nm}$ . In some cases, signals we actually measure may be generated at depths as great as  $10\mu$ . If this is so, how can we ever achieve information with detail approaching that of the initial spot size? One example of high resolution information is obtained from secondary electron emission, comprised of electrons which have very low energies. Owing to their extremely low energies, secondary electrons that are generated at depth simply don't have sufficient energy to leave the specimen. Only those secondary electrons generated very close to the surface, where the interaction volume is small (approaching that of the initial spot size), have any chance of escaping and being detected.

For emissions that occur throughout the interaction volume and yet can still be detected at the sample surface, we can reduce the size of the volume from which that information is generated by reducing the energy of the primary electron beam. For example, a  $15\text{keV}$  electron beam will produce an interaction volume of several cubic microns or more, however, in the same material, a  $10\text{keV}$  electron beam will produce an interaction volume of approximately  $\frac{1}{2}$  a cubic micron. Of course the intensity of the emissions will be significantly reduced at the lower energy, especially for characteristic x-rays of moderate energy.

Recall that the *Heisenberg Uncertainty Principle* states that it is impossible to simultaneously describe the position and energy of atomic particles. We must therefore treat electron interactions and scattering events in terms of probabilities. If we consider any type of event possible within the target, the probability of it occurring is given in units of area, or cross-section,  $Q$ . When we refer to someone's ability to "*hit the broadside of a barn*", we are actually talking about probability, and it is not coincidental that we speak of scattering probabilities in terms of "*barns*" of finite size (ca.  $10^{-24}\text{cm}^2/\text{nucleus}$ ). Think of an element's cross-section as the effective size of an atom associated with a particular event. Historically these atomic cross-sections have been empirically measured from a known volume of possible event sites, and then differentiated with respect to depth and the number of incident electrons.

---

<sup>1</sup> Magnification in this sense is different from optical microscopy in that magnification is achieved by reducing the area scanned on the target while the viewing area remains constant. In this sense it is possible to reduce the area on the target beyond the detail capable of the spot size, resulting in magnified fuzziness. Practical magnifications should be judged relative to the resolution the eye can discern, say, 7 lines per mm at 2 feet distant. If we were to apply this criteria to a  $10\text{cm}$  square photo, then a horizontal line would be made up of 700 discernible spots. If the spot size was  $10\text{nm}$  then the linear dimension on the magnified target would be 7 microns, and the magnification would be  $100,000/7$  (photo microns/target microns), or 14300x.

Primary-beam electrons have energies greatly exceeding the amount of energy lost in a typical scattering event. Hence individual beam electrons will undergo numerous scattering events, each with their own probabilities. Between these events, the electron travels through the specimen. It should be obvious that one of the most important factors is the path length between scattering events. The *mean free path*,  $\Gamma$  (cm) between events is calculated from the following equation:

$$\text{mean free path } (\Gamma) = \frac{A}{N_o \rho Q}$$

eq. 2-1

where  $A$  is the atomic weight,  $N_o$ , is Avogadro's number and  $\rho$  is the density.

Since we are talking about many types of events and cross-sections, the distances between them need to be determined for each type. The *total mean free path* is calculated as

$$\frac{1}{\Gamma_{ave}} = \frac{1}{\Gamma_a} + \frac{1}{\Gamma_b} + \frac{1}{\Gamma_c} + \dots$$

eq. 2-2

Nowadays, computer software is routinely used to simulate scattering events, path lengths and directions, and the generation of different energy forms that we might actually observe during electron beam interaction. Because of the probability-based nature of these processes, the computations typically involve *Monte Carlo* simulations. Some typical Monte Carlo simulations are illustrated in Figures 2-1, 2-3 and 2-4 of this chapter.

## 2.1 Elastic scattering

As defined above, this type of event gives up little energy to the target, but is likely to significantly modify a primary electron's trajectory. The energy of the primary electron, typically thousands of volts, is associated with its velocity (i.e., kinetic energy). During an elastic scattering event the electron's energy loss is likely to be measured in volts. The probability for large deviations in trajectory is directly related to the atomic number of the target, and inversely to the electron's energy.

$$Q_{>\phi_0} \propto \frac{Z^2}{E^2}$$

eq. 2-3

Equation (2.3) describes the probability of a deviation greater than a certain angle as a function of atomic number and electron energy. The relationship is intuitive. If you can imagine electrons of a given energy, "bouncing" off atoms which differ in atomic number; the primary electron will deviate a greater degree if affected by a high- $Z$  element containing a large number of electrons (a dense electron cloud) surrounding the nucleus. Conversely, highly energetic electrons are less likely to be deflected than electrons with lower energy. If these

deflected electrons escape the target, the number of electrons detected will have an atomic number dependence, which can be informative for specimens like petrologic thin-sections. This is the origin of backscattered electrons.

Elastic scattering is also important to us because the amount of information we may gain from inelastic scattering events is directly related to how much energy remains after elastic scattering. If, for example, a highly energetic, primary electron is scattered very near the point of impact with the target, and then escapes from the target, that electron is no longer capable of transferring any of its energy to the specimen. It is therefore no longer available to generate x-rays, and is an important consideration if we want to model the interaction volume as a function of composition.

## 2.2 Inelastic scattering

This type of scattering event exchanges significant amounts of energy with the target. Depending on the amount of energy exchanged, there is a spectrum of energy released during these events. The energy released in such an event is a function of the quantum state of each atom involved, and hence is target dependent. A brief description follows for the different types of information important to us.

*Plasmon excitation* is the most common form of energy transfer, but it turns out to be rather uninformative for our purposes. It is analogous to throwing a rock into a pond; the water molecules close to the "event" are affected directly, but the whole pond feels the pressure wave. The event is generally attributed to exciting waves in the "free electron gas". The cross-section for plasmon scattering is large and so it is highly probable, but the energy exchange is small, typically 5 to 30 volts.

*Phonon excitation* results from the primary electrons interacting with the target's bonding structure -- the crystal lattice in the case of minerals. The end result is localized heating caused by structural vibration. This is usually no more than a side effect because the heat production is so localized (several cubic microns) and because most specimens are able to dissipate the heat so that a temperature increase of 10 degrees (C) is generally a maximum. There are cases, however, for which care should be taken. These include biological materials which can not withstand even this small temperature increase. Another potential problem exists in materials with relatively weak ionic bonding. The best example involves Na—O bonds, where increased thermal vibration may actually destroy the bond and allow the ions to "migrate". If the ions are attracted to a space charge, then they may actually leave the interaction volume. Sodium will migrate by diffusion toward a negative space charge, and oxygen will sometimes "boil" from the surface. The sodium migrates out of the interaction volume, and thus produces a decreasing number of Na x-rays measured over time. This effect is severe for amorphous specimens (e.g., Na in volcanic glass)! It is unnoticeable for tightly coordinated Na-bearing minerals such as jadeite. Between these two extremes the severity of the problem is variable. Most noteworthy is the analysis of feldspars that requires recognition of Na-loss as a potential problem. This effect is dependent on the energy used for the primary beam of electrons, and on the *beam current* (the number of electrons per time interacting within

the target). For a given energy and beam current, the effect can be reduced by increasing the spot size. Several of you may encounter this problem in your project work and require the use of a volatile element correction in the acquisition software.

**Conduction band electron excitation** is the process for generating what are termed *secondary electrons*. Conduction band electrons are easily perturbed by the energetic primary electrons, but because they are loosely held, little energy is exchanged and secondary electrons produced in this process typically have energies in the range of 1 to 50 volts. The majority of these electrons usually have a velocity equivalent to less than 5 volts, and such extremely low-energy electrons can't travel very far. Secondary electrons generated within about 5nm of the surface are the only ones with a significant chance of leaving the target, and it is because of this that we are able to achieve a high degree of detail/resolution with the SE signal. Because secondary electrons are generated from sites differing in degrees "held", (e.g., conduction bands, outer covalent bands, etc.), we can sometimes discern and make a distinction between *slow* and *fast* secondaries. The fast secondaries will be generated with as high as 1000 volt velocities, and have been measured to have trajectories generally normal to the incident electrons. Their fraction of the SE emission is small but they can degrade the detail normally attributable to a SE signal, so if possible, instrument parameters or specimen preparation should be used to minimize the effect. For example, coating the non-conducting target with a metal would increase the conduction/covalent bond ratio, and should reduce the effects due to fast secondaries. This is one reason why we coat specimens with a layer of gold if we are interested in maximizing the resolution for imaging with secondary electrons.

**Ionization of inner shell electrons** can occur if a primary electron has enough energy to "knock out" an electron from one of the tightly held inner atomic shells (orbitals). If this occurs the atom is said to be ionized, and will be highly unstable. It will stabilize by transferring an electron from a higher shell to the electron hole, and in doing so will emit characteristic radiation in the spectrum of x-ray energies. It is this event we will be primarily concerned with regarding x-ray analysis (see the chapter *The Nature of X-rays*).

**Bremsstrahlung or Continuum x-rays** are generated from the primary electron's interaction with the strong coulombic field of an atom. The energy loss from this process is released as Bremsstrahlung or "braking radiation". These are x-rays with energies throughout the spectrum, a continuum limited only by the energy of the primary electron beam,  $E_0$ . The end result will be a broad band of x-rays which is the primary contribution to noise or background when measuring characteristic x-rays.<sup>2</sup> This background is very important because care needs to be taken to subtract it properly from the x-ray intensity we are trying to measure; and it is likely to be very different from one target to the next. In addition the highest energy continuum emissions produced can also be utilized as a very accurate method to determine the

---

<sup>2</sup> It is instructive to point out here that x-rays themselves can ionize these inner shells; this type of ionization is termed *fluorescence*. If x-rays are the sole means by which characteristic x-rays are generated there will be no bremsstrahlung, and if we make a comparison with the *x-ray fluorescence* analytical technique, it is this continuum radiation due to particle interaction which distinguishes the two types of x-ray generation, allowing the fluorescence technique to be much more free of background *noise* and therefore more sensitive to trace element concentrations.

actual energy of the primary beam since no continuum x-rays can be produced with an energy greater than the primary electron beam.

Inelastic scattering constantly reduces the energy of a primary electron, finally to the point at which it is "captured". At this point it is instructive to examine the energy loss quantitatively, as a function of distance traveled, and also as a function of target composition. There are an infinite number of target compositions, however they all can be grouped and studied as a function of average atomic number ( $Z$ ), atomic weight ( $A$ ) and density ( $\rho$ ). Bethe (1933) first derived the *continuous energy loss* relationship for all inelastic scattering possibilities. The energy loss per unit of distance traveled by an electron,  $dE/dx$ , is approximated by the following equation:

$$\frac{dE}{dx} = 2\pi e^2 N_0 \frac{Z\rho}{AE_m} \ln\left(\frac{1.166 E_m}{J}\right)$$

eq. 2-4

where  $e$  is the charge on the electron,  $N_0$  is Avogadro's number,  $E_m$  is the mean electron energy, and  $J$  is a function of atomic number:

$$J = (9.76Z + 58.5 Z^{0.19}) 10^3 \text{ keV}$$

eq. 2-5

A concept related to the continuous energy loss approximation is the density normalized *stopping power* for a target:

$$S = \frac{1}{\rho} \frac{dE}{dx}$$

eq. 2-6

For target density normalized stopping power, the Bethe equation is reduced to the proportionality,

$$S \propto \left(\frac{Z}{A}\right) \ln\left(\frac{c}{f(Z)}\right)$$

eq. 2-7

where  $c$  is a constant. It is interesting to point out that stopping power decreases with increasing atomic number, and it shouldn't be confused with the backscattering properties of a target. For the most part the confusion arises simply from having conveniently defined *stopping power* as density normalized; i.e., inversely related to density. It is also misleading if we make comparisons between inelastic and elastic types of events.

## 2.3 The interaction volume

The *interaction volume* is controlled by both elastic and inelastic scattering. Depending on the target composition, one or the other may predominate at any point in the trajectory. Consider a low-atomic-number target where elastic scattering will be at a minimum for the high energy electron beam. The primary electrons will enter into the target without deflecting until inelastic scattering has reduced their energy such that elastic scattering is now a significant process. The resultant volume will be narrow at the entrance, and become "bulbous" at depth. This "pear-shaped" volume is characteristic for most targets, with the exception of high-atomic-number targets (e.g., tantalum or gold) where elastic scattering is initially significant. Figure 2-1 depicts a single electron's path in low and high atomic number targets. Notice elastic scattering isn't significant until late for the low-Z target, whereas for high Z, on entry elastic scattering plays a much more significant role.

As you examine the scattering character for both of these targets, and notice the effect that elastic scattering has on the volume, it should be apparent that if both of the metals were alloyed into a single homogeneous phase, the character, as well as the volume, would be a result of the scattering contribution from both of the elements in the sample interaction volume. Many of the emitted productions that we have described can be calculated for multi-element compounds by the use of the concept of the average atomic number.

This is a hypothetical number that attempts to describe the average property of a material by calculating the contribution to that property from each different atom in the sample and relating it to an "averaged" atomic number. Traditionally this is normally calculated for many of the properties that we have discussed using the following expression,

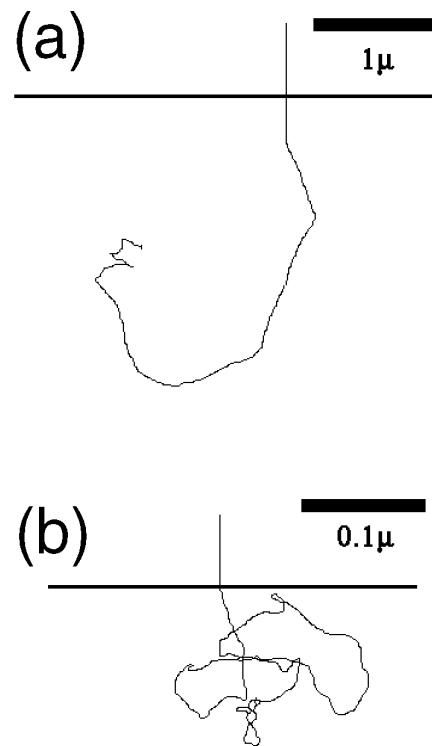


Figure 2-1 Monte Carlo simulation of a single 15keV electron in metallic (a) silicon and (b) gold. Note the scale. (D. Joy software)

$$\bar{Z} = \sum_i C_i Z_i$$

eq. 2-8

where  $C_i$  is the element's weight fraction. This relationship holds for virtually all of the properties we will discuss in this course. For example, properties that utilize mass normalized parameters, such as mass absorption coefficients, are correctly calculated by summing the mass fraction pure element property for each element in the material. For other properties, such as continuum x-ray and backscatter yields, there is no *a priori* reason to assume that they can be averaged by mass fractions. This is still an area of controversy in the field today and is discussed in some detail in the following papers:

Donovan, J. J. and Pingitore, N. E., "Compositional Averaging of Continuum Intensities in Multi-Element Compounds", *Microscopy and Microanalysis*, 2002, v. 8, 429-436

Donovan, J. J., Pingitore, N. E. and Westphal, A. N., "Compositional Averaging of Backscatter Intensities in Compounds", *Microscopy and Microanalysis*, 2003, v. 9, 202-215

The shape of an interaction volume should not be imagined in an absolute sense. As can be seen by the simulated interaction paths, above or those below, the *interaction volume's* edge is difficult to determine precisely. As alluded to above, a typical volume diameter might be given as  $1\mu$ . This dimension was in the context of x-ray generation, but did we mean all x-rays or some x-rays? The context was also with respect to resolution, which would imply distinct volumes, measured separately from the other. Statistically however, such volumes do not have to be entirely separate to be distinct. The volumes can overlap and still give off distinct information; all that we might establish are criteria that the information be statistically different. With regard to x-rays, we might establish such criteria analogous to the sigma ( $\sigma$ ) value we associate with measured data, i.e., the measured value is good within a range of values considered the possible error ( $\pm\sigma$ ). This given range ( $\pm 1\sigma$ ) is said to contain 68% of all possibilities, whereas  $\pm 2\sigma$  would contain 95%, and  $\pm 2.85\sigma$  would contain 99%. When a volume dimension is spoken of with respect to x-ray generation, it is in the context of similar statistics, and is generally the volume in which  $1\sigma$  of all x-rays are generated. Clearly a volume containing 70% of the information could be said to be distinct from the neighboring volume,

but one should be careful when analyzing small volumes, because, clearly, not all of the x-rays are coming from the dimension we are claiming to be distinct. If we speak of the volume that contributes to the information, then for absolute (99.5%) certainty, we should be multiplying by three ( $3\sigma$ ).

Another way of imagining the interaction volume's dimension is with respect to the expenditure of the primary electrons' energy. Figure 2-2

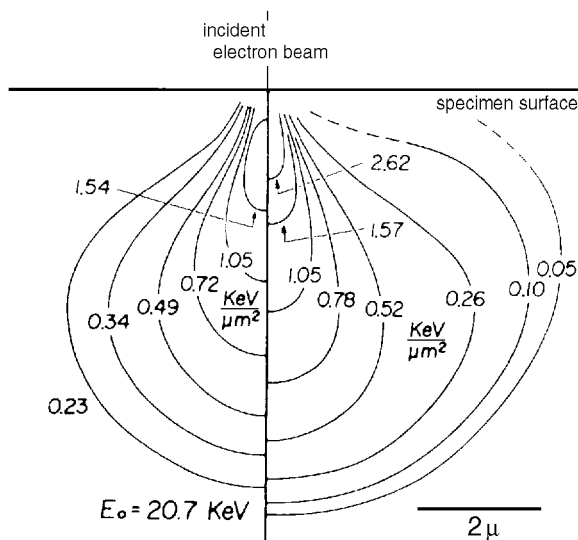


Figure 2-2 Energy expenditure in a low Z target. (left) Monte Carlo simulation, (right) experimental etching of PMMA. (after Everhart, et al., 1972)

describes the volume relative to energy expenditure, for (1) (left) a Monte Carlo simulation, and (2) (right) for an empirical study of exposing plastic to an electron beam and then etching to reveal the disturbed volume.

Monte Carlo simulations offer a tool by which we can qualitatively, sometimes quantitatively, evaluate the effects of electron beam energy, atomic number and incident angle on the size and shape of the interaction volume. These simulations trace step-by-step the history of an electron in the target until it is captured. Elastic or inelastic events are predicted, from one possible event site to another, with the calculated average mean path between; if inelastic, then ionizations may be predicted, and subsequent energy loss to the electron calculated, and so on. For these simulations to be statistically significant, the modeled volumes should be generated with thousands of primary particles. This can use a lot of computer time, and as the number of simulated paths becomes large, the individual paths become obliterated.

To give you an idea of how the Monte Carlo simulations relate to the real conditions taking place in the instrument, consider the following: **if the models were made up of one million particle paths, it would still only be the equivalent of approximately one ten millionth of a second of interaction within an actual specimen** (calculation based on 10 nanoAmps (nA) beam current).<sup>3</sup> On the other hand, a calculation involving one million trajectories has relative precision errors on the order of 0.1%, even though the accuracy errors

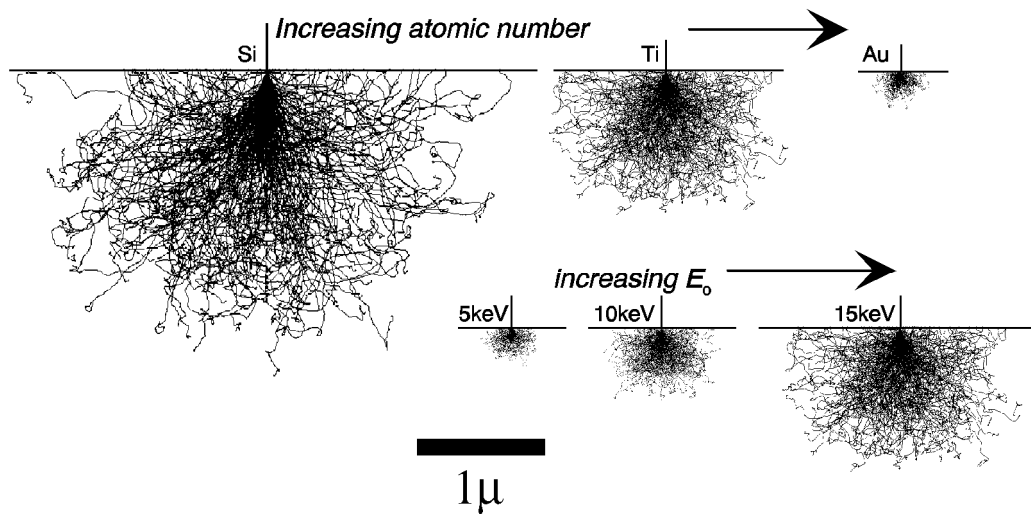


Figure 2-3 Monte Carlo simulation showing the interaction volume's size as a function of target composition (increasing  $Z$ , top), and increasing acceleration voltage,  $E_0$  (bottom). Calculated with software from D.C. Joy (1991).

are probably much larger.

<sup>3</sup> The *beam current* should be considered a measure of how many electrons are interacting with the target, independent of the acceleration voltage. It is usually measured by collecting the beam in a *faraday cup*, and its magnitude is generally 1 to 100 nanoAmps (nA). Its variation does not affect the character of the scattering, only the number of events per time. However, if an effect such as heat, which is a function of the number of events, can change the properties of the target, e.g., density, the scattering character might change with time.

Figure 2-3 is a collection of Monte Carlo simulations for 250 electron scattering paths in targets of varying atomic number (constant beam energy, 15keV), and for varying beam energy (constant target composition, Ti). Trajectories that leave the specimen represent backscattered electrons. While each particle's path is shown until completion, you should recognize that information from inelastic scattering isn't generated near the "death" of the electron because late in its interaction history it doesn't have enough energy for an informative event to occur. For inner shell ionizations, the volume that encloses sites of x-ray emission is considerably smaller. If you consider x-ray generation from different elements, the volume might be larger or smaller as a function of how much energy it takes to ionize the inner electron

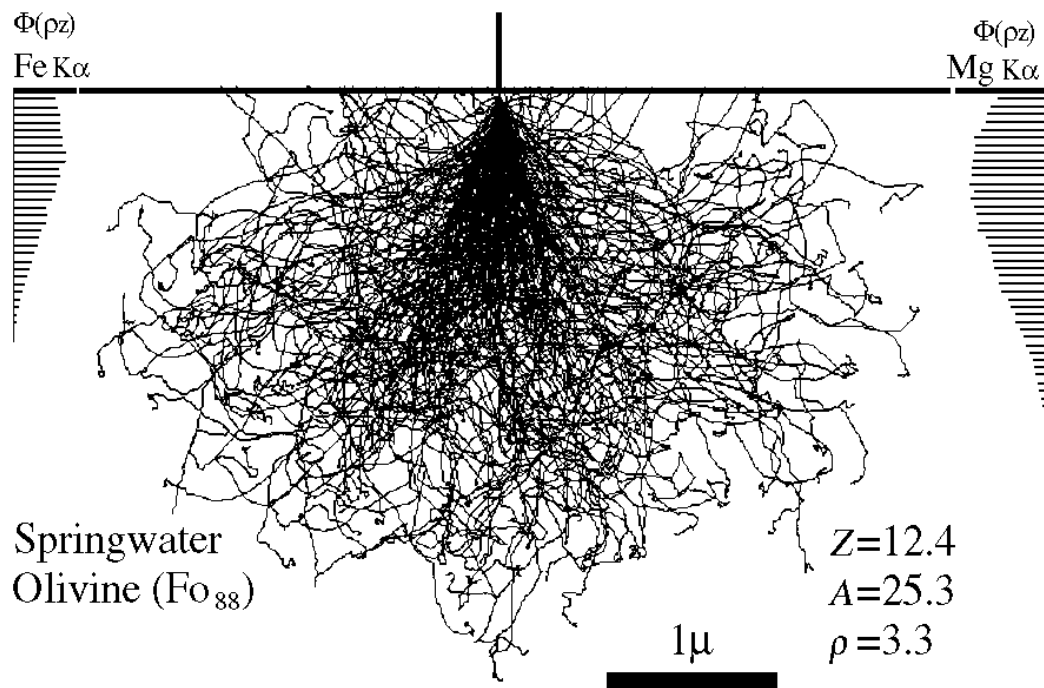


Figure 2-4 Monte Carlo simulation for 15keV electrons in olivine (Fo80).  $\Phi(\rho z)$  distributions are shown for Fe (left) and Mg (right). Why is the depth of Fe generation shallower? Calculated with software from D.C. Joy (1991) shells of different atoms.

Figure 2-4 is a Monte Carlo simulation for 15keV electrons in an olivine, which also shows the depth distribution histograms for Mg and Fe Ka x-ray generation, known as  $\Phi(\rho z)$  curves.<sup>4</sup> Notice that Mg present in the olivine is sampled at greater depths than is Fe.

Finally, the last thing we should mention about x-ray production (it will be taken up in depth later) regards the  $\Phi(\rho z)$  curves that describe the depth for generation of x-rays. We should make a distinction here between generation of x-rays and emission, because the latter takes into account absorption along the path to the detector. As we will see later, the atomic number factor for correcting x-ray information is concerned with the volume in which x-rays

<sup>4</sup>  $\Phi$  is the distribution histogram, the shape of which is a function of density and depth ( $\rho z$ ).

are generated, and the absorption and fluorescence factors describe the attenuation and enhancement effects for the x-rays actually emitted from the target.

## 2.4 Backscattered electrons

Backscattered electrons are one of three types of electrons emitted from the target: backscattered, secondary and Augér. *Augér* electrons will be briefly mentioned later in the context of x-ray generation, but are largely beyond the scope of this text. Figure 2-5 depicts the energy spectrum of secondary and backscattered electrons. This figure depicts the energies of all the electrons that would be detected coming off the surface of material being bombarded by a high-energy beam of primary electrons. It clearly shows the bi-modal distinction between the high-energy backscattered electrons and the low-energy secondary electrons.

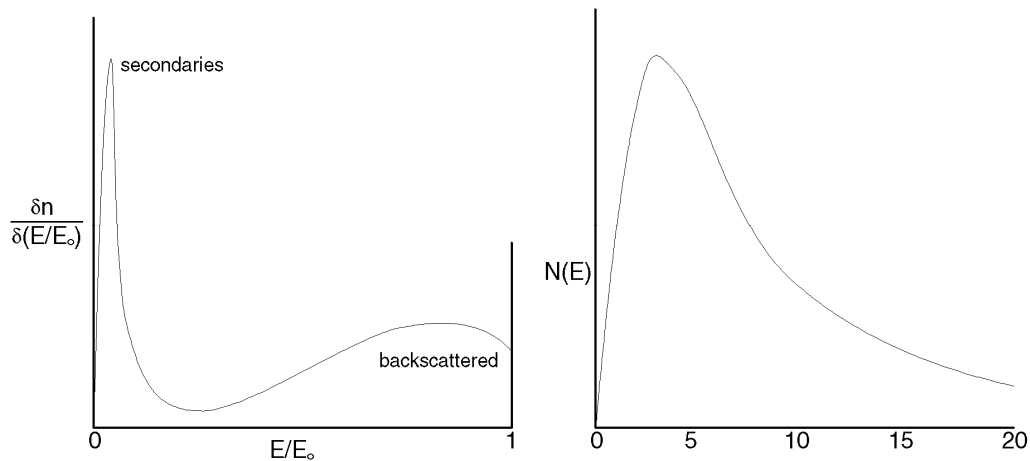


Figure 2-5 Energy distribution for electrons emitted from the target. Entire spectrum (left), and expanded spectrum of the energy distribution for secondary electrons (right). (from Goldstein, et al., 1981)

Notice that backscattered electrons exhibit a wide range of energies, but the peak of BSE emission is very close to  $E_0$ . As noted earlier in this chapter, backscattered electrons are produced when primary-beam electrons are scattered in such a direction that they leave the target entirely. Beam electrons that undergo elastic scattering close to the point of impact and leave the specimen will not have had their energies significantly reduced by inelastic scattering and hence produce BSE with energies only slightly below that of the primary beam. The low-energy range of BSE is produced by primary electrons that have undergone multiple elastic and inelastic scattering events, and thus have lost much of their original energy before leaving the surface of the specimen.

The phenomenon of backscattering has been studied experimentally by applying a 50V potential to the target so secondary electrons won't escape from the surface, and carefully

measuring the beam current and comparing it to the specimen current<sup>5</sup>. The difference between the two measured currents is a measure of lost electrons due to backscattering.

The fraction of incident-beam electrons that are backscattered is called the **backscattering coefficient**, and is represented by the Greek letter "eta" ( $\eta$ ). As shown in Figure 2-6, the fraction of electrons backscattered, and the distribution of BSE energy varies significantly with atomic number. BSE emission can be as much as 50% of the primary incident current depending on the atomic number,  $Z$ . The BSE signal when used for imaging can be very informative if the analyst has an understanding of backscattering relative to instrumental parameters and target properties.

Not only is it important to know the fraction of BSE ( $\eta$ ), but for quantitative calculations we must also consider their energy distribution. This is because the BSE with high energies would have been more likely to excite a particular x-ray line (i.e., would have produced a higher count of x-ray photons per second) than lower energy BSE. The probability of exciting any x-ray line with  $E_C$  excitation energy goes down to zero obviously for BSE with  $E < E_C$ . The energy distribution within the BSE fraction is usually expressed in terms of the differential fraction of BSE. The fraction backscattered per unit interval of energy at constant primary beam energy ( $\delta\eta/\delta W$ ) {where  $W$  refers to the normalized energy,  $W = E/E_0$ } is plotted against the normalized energy (Figures 2-5 and 2-6). Several features of Figure 2-6 should be noted.

- (1) The normalized energy ( $E/E_0$ ) is used because the **shape** of the energy distribution does not change very much with  $E_0$ . Plotting the energy distribution against  $W=E/E_0$  eliminates the need for the second variable (i.e., eliminates the need to plot a family of curves of  $\delta\eta/\delta E$  vs.  $E$  for different values of  $E_0$ ). Instead, one curve of  $\delta\eta/\delta W$  vs.  $W$  is valid for all  $E_0$  and contains the same information.
- (2) The area under the curves between any two limits of  $W$  represents the BSE fraction in

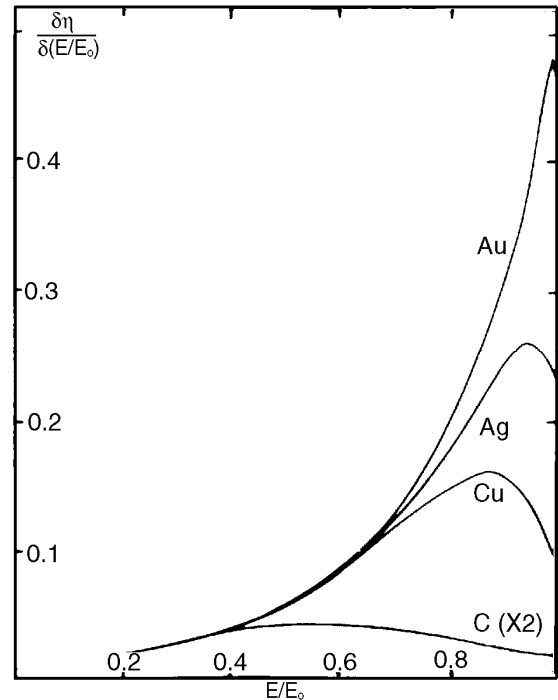


Figure 2-6 Backscattered electron emission as a function of atomic number (the curve for C is multiplied by 2). (from Goldstein, et al., 1981)

<sup>5</sup> SEM users sometimes use the terms *beam current* and *specimen current* interchangeably, because reporting the approximate current used is generally enough. However, in the context of quantitative EPMA, we should make a distinction because the current used is an instrumental parameter which needs to be maintained accurately over a period of hours, from one session to another, as well as reported. Both terms would be equal if the *specimen current* (measured between the specimen and ground potential) was captured in a *Faraday cup* in place of the specimen. In most probes today this is a cup that is inserted into the beam's path; in older instruments it was a calibrated aperture that sampled the outer regions of the beam above the objective lens.

that particular energy range. For example,

$$\int_W^{(W+dW)} \left( \frac{\delta\eta}{\delta W} \right) dW = d\eta$$

eq. 2-9

where  $\delta\eta \equiv$  the BSE fraction coming off with energies in the interval  $W$  to  $(W+dW)$ .

(3) The maxima of the curves correspond to the most common energy of the BSE. For very light elements such as carbon the maximum is very broad (i.e., the energies are almost evenly distributed) and occurs roughly at  $W = 0.5$  or  $E = E_0/2$ . For all elements heavier than C, the maximum is skewed towards  $E_0$  or  $W = 1$ . For example, the most common energy from a target with a mean atomic number of 29 is  $W = 0.89$  or 13.4keV for  $E_0 = 15$ keV.  $E_{\max}$  increases with mean  $Z$ .

(4) The total area under the curves,  $\int_0^1 (\delta\eta/\delta W)dW$ , is equal to the total BSE fraction,  $h$ .

Elastic scattering, which is responsible for backscattering, is directly proportional to the target's mean atomic number, and inversely proportional to the beam energy. Figure 2-7 is a plot of experimentally determined backscatter coefficients as a function of atomic number for two very different primary energies ( $E_0$ ). Notice the very small difference between the two curves (an extreme of 10 and 49keV). Such a plot emphasizes the fact that  **$h$  is strongly dependent on  $Z$ , but only weakly dependent on the beam energy**. For minerals with mean atomic numbers in the range most petrologists are interested in ( $Z=10$  to 35), the curve is the steepest, and contrast between various phases and compositions should be very good. These data can be fit to the general equation:

$$\eta = 0.0254 + 0.016Z + 1.86 \times 10^{-4} Z^2 + 8.3 \times 10^{-7} Z^3$$

eq. 2-10

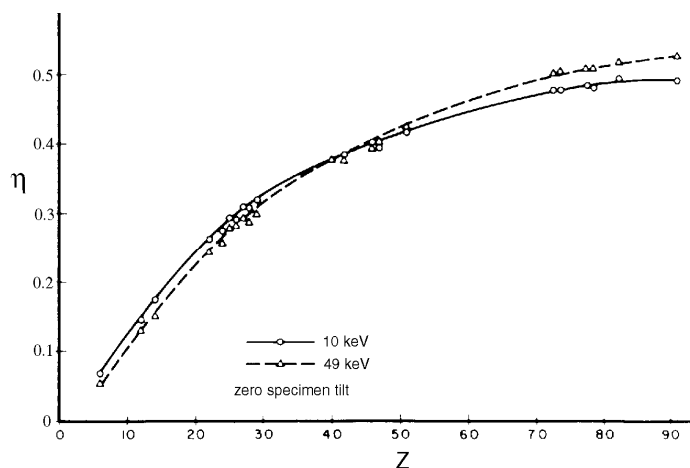


Figure 2-7 The backscatter coefficient,  $\eta$ , as a function of atomic number for primary acceleration voltages of 10 and 49keV. (from Goldstein, et al., 1981)

Today, BSE detector manufacturers claim discernible image contrast between compositional differences of 0.1Z, which is approximately the difference between forsterite<sub>84</sub> and forsterite<sub>85</sub>. Examples of BSE images are shown in Figures 2-8 and 2-9.

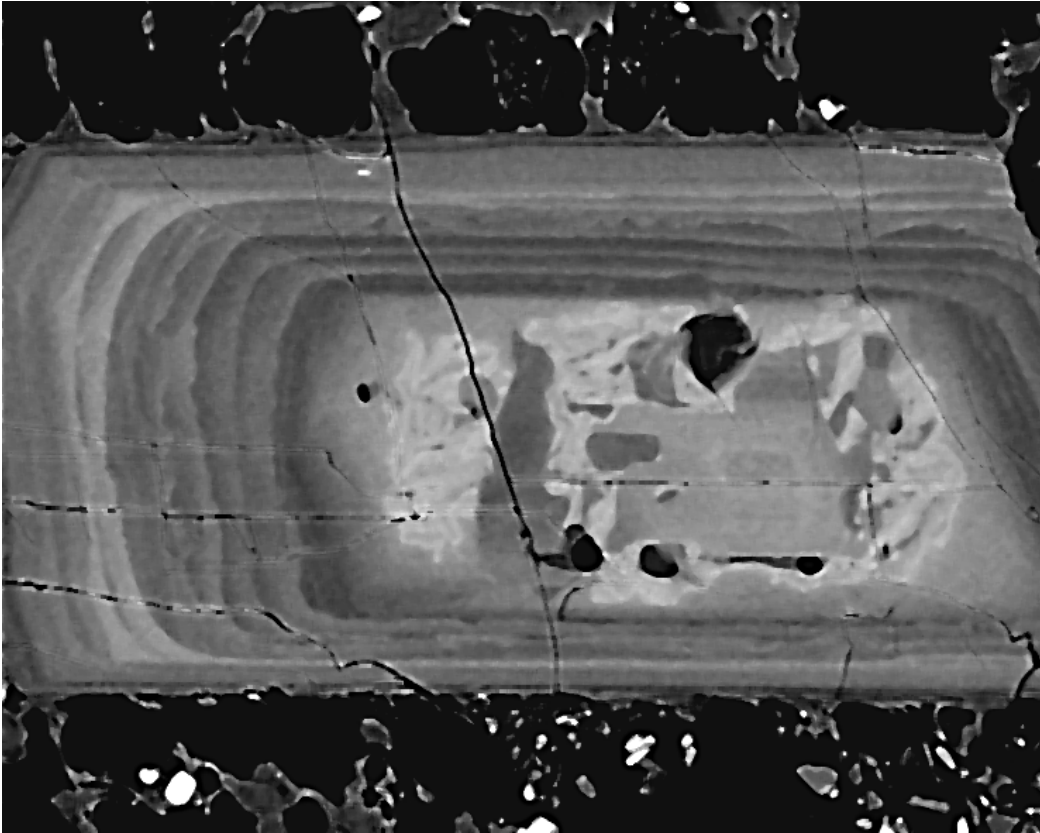


Figure 2-8 BSE image of zoned a plagioclase phenocryst from the Mt. St. Helens dome. Darker regions correspond to areas enriched in the albite (sodium) endmember; and brighter areas are enriched in the anorthite (calcium) endmember.

## 2.5 Secondary electrons

Secondary electrons are generated when primary beam electrons strike or perturb conduction band or weak electrons. As Figure 2-5 illustrates, the total electron emission from a target being bombarded by high-energy electrons is bimodal. The low energy distribution of electrons is produced by secondary electrons (SE). The arbitrary cutoff between the low-energy end of the BSE spectrum and the high-energy end of the SE spectrum has been historically defined as 50 volts, however more recent studies such as Figure 2-5 indicate that secondary electrons rarely exceed 10V with a maximum peak at less than 5 volts.

Low-energy secondary electrons are very useful for producing images of surface topography because:

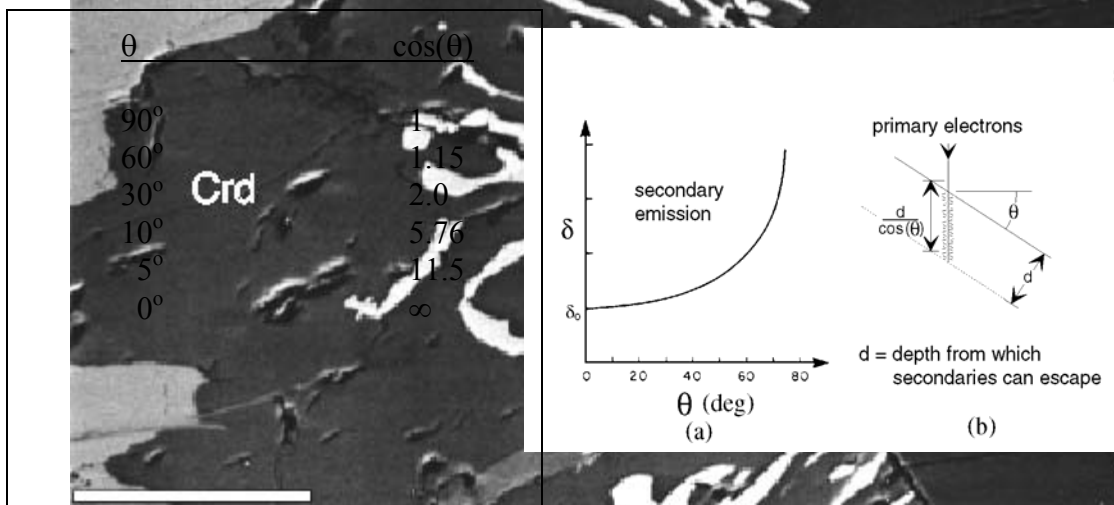


Figure 2-9 BSE image of metamorphic symplectite (left) and a graph showing the relationship between angle and depth (right). The symplectite consists of cordierite (dark gray) and hegyrta (white). Secondary electrons.

- 1) The maximum distance beneath the surface from which they can actually be emitted is very small (typically a few nanometers), even though low-energy secondary electrons are produced in the sample throughout the entire interaction volume (typically several cubic microns). This depth limitation arises from the fact that secondary electrons are rapidly absorbed by the specimen because of their very low energies.
- 2) Within this shallow depth range of effective production of low-energy secondary electrons, the primary beam has suffered very little lateral "spread" by high angle scattering events. Therefore, the origin of the secondaries for a given electron beam position on the sample is very close to the surface at the point of beam impact, and the secondary electron signal contains information about the surface with a spatial resolution comparable to the diameter of the electron beam (ca., 5nm).
- 3) Unlike the situation with BSE, **the yield of SE (i.e., the strength of the signal), does not vary much with Z, but depends strongly on the angle between the beam and the surface of the target at the point of impact.** Therefore the intensity of the emitted signal is strongly correlated to topographic information (specimen shape).

The qualitative reason for this is simple to understand and is illustrated in Figure 2-10. Let  $d$  be the maximum distance within the sample from which SE can travel and reach the surface with sufficient energy to be emitted (i.e.,  $d$  defines the depth of the skin layer that the secondary electron signal can come from). Since  $d$  is only a small fraction of the total depth of penetration of the primary beam electrons, the latter will have energies close to  $E_0$  and will not have deviated from their original direction as they travel through layer  $d$ . As a result, the yield of SE will be proportional to the length ( $L$ ) of the path traveled through this layer by the primaries (i.e., the longer the path through layer  $d$  the greater the number of secondary electron producing events).

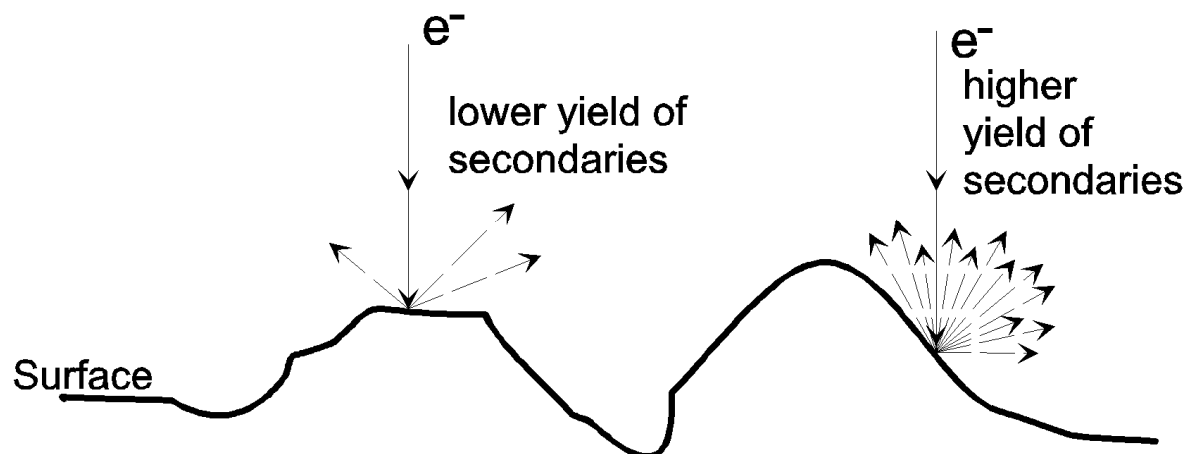


Figure 2-11 Secondary electron emission from a rough specimen. Increased image brightness is the result of increased electron emission when the electron beam interacts at shallow angles (e.g., right).

Figure 2-10 and its accompanying table illustrate that the number of SE that will be collected by a detector situated above the specimen will be dominantly controlled by the surface topography. In other words, the strength of the SE signal will be related to the slope of the specimen surface lying directly under the beam at any point in time; i.e., inversely proportional to the cosine of the interaction angle. This concept is reinforced in Figure 2-11. If the beam is scanned over a "rough" surface, the slopes will appear bright and the flat areas will appear dark.

SE are generated as the primary electrons interact with, and perturb, conduction band electrons. Such an event is inelastic, and reduces the primary electron's energy by a very small amount. As we have seen, backscattered electrons can be as energetic as primary electrons, and we should suspect that SEs could be generated by BSEs as well. This implies that a contribution to the SE signal could be due to a backscattered electron as it leaves the target, some distance away from the small volume we normally attribute to SE emission. If this is so, what is the BSE contribution to degrading SE image resolution?

As we did earlier with BSE, let's introduce another coefficient for SE production,  $\delta$ ,

$$\delta = \frac{n_{SE}}{n_{beam}} = \frac{i_{SE}}{i_{beam}} \tag{eq. 2-11}$$

If we also consider the BSE influence,

$$\delta_{total} = \delta_{SE} + \eta \delta_{BSE} \tag{eq. 2-12}$$

where  $\eta$  is the backscatter coefficient. The simple ratio of  $\delta_{BSE}/\delta_{SE}$  has been experimentally determined to be on the order of 3 or 4, implying that the generation of SE with BSE is more

efficient than with primary electrons. This is because BSE generally leave the target at shallower angles than the primaries enter the target, thus allowing more interactions along a BSE path within the depth for which SE can be generated and escape. Also, since BSE have less energy than the primaries, the SE-generation event's cross section is larger. At first glance, this might imply that SE resolution should be severely degraded by the contribution of SE generation by BSE. This potential problem is alleviated somewhat by including the backscattering coefficient ( $\eta$ ) which reduces the number of BSE capable of generating SE, and reduces the ratio of  $\delta_{\text{BSE}}/\delta_{\text{SE}}$  to about 1.

More importantly, when the primary beam strikes the target at a significant angle (due to surface topography or specimen tilt) the path length through the surface layer capable of producing SE is greatly increased relative to that traveled by the backscattered electrons (thereby increasing further the contribution of the primary beam and hence the resolution). What this all means is that SE imaging of specimens (or small areas within specimens), which are flat and normal to the beam, will have the SE image resolution degraded by the contribution from the BSE. In order to compensate for this feature, modern SEM instruments provide the capability to **tilt** the specimen relative to the primary beam. This capability not only improves the resolution but also provides the opportunity to view more of the three-dimensional character of the specimen.

Although the majority of secondary electrons originate in the conduction band, it is possible for primary-beam electrons to "knock-out" outer valence electrons as well. Such electrons will have considerably higher energies - up to 1000 volts - and are often called "*fast secondaries*". The effect of producing fast secondaries is to degrade the resolution of the SE image. One way to overcome this problem is to coat the specimen with a thin layer of material that contains a large number of conduction-band electrons, thereby greatly increasing the ratio of conduction-band to valence-band electrons. If the conducting coat is greater than 5-10nm in thickness then all of the SE are produced within the surface coating rather than within the specimen itself. Materials possessing the desired properties and are suitable for coating include elements such as platinum and gold, and to a lesser degree, carbon.

Although the generation of secondary electrons is not strongly dependent on  $Z$ , there is a noticeable increase in production for targets  $Z=6$  to  $Z=14$ . At higher atomic numbers, SE production is virtually independent of  $Z$ . Therefore, if we are interested in maximizing the resolution and contrast for SE imaging of non-conducting specimens, the coating of choice is gold. In our lab, we commonly coat specimens for SE imaging with a layer of gold approximately 200 angstroms (20nm) in thickness. Thinner layers are not really possible because the coating process tends to deposit the gold as "islands" which must coalesce before being truly conductive. A 20nm thick layer of gold obviously interferes with x-ray analysis, so in cases where we want to analyze the chemical composition of the material or use x-rays for imaging, we coat the specimen with carbon. The choice of carbon is strictly for the sake of x-ray analysis because it contributes nothing to the spectrum of interest, but as well, contributes nothing to the SE signal. The character of its layer is however more conductive for a thin layer, as evaporation of carbon tends to lay down a more uniform layer.

## 2.6 Magnification and Depth of Field

One of the most significant advantages of SEM imaging of topography is the combination of relatively high magnification and generous depth of field (see also chapter *Electron Beam and Electron Optics*). The magnification of images in electron beam instruments is determined by the ratio of the size of the image displayed on either a CRT or a photograph (fixed for a given instrument) to the size of the area scanned on the sample (a variable). Two examples:

- (1) a  $200 \times 10^{-6}$  m ( $200\mu\text{m}$ ) scan displayed on a  $20 \times 10^{-2}$  m (20cm) CRT screen gives a magnification of 1000X.
- (2) a  $100 \times 10^{-6}$  m ( $100\mu\text{m}$ ) scan displayed on a  $20 \times 10^{-2}$  m (20cm) CRT screen gives a magnification of 2000X.

The practical range of the magnification for the SEM is generally 20 to 100,000X versus 20 to 1,000X for the optical (light) microscope.

The *depth of field* in a microscope is similar to a camera, and may be defined as the maximum distance measured along the optical axis for which the specimen remains in acceptable focus by an eye observing the image. The depth of field is directly related to the angular aperture of the lower lens (objective lens) in the system. The larger the angular aperture of the objective lens, the shallower will be the depth of field. This relationship is illustrated in the next figure.

This sketch applies to the light microscope as well as to the SEM, although there are fundamental differences between the image-forming processes in the two types of microscopes. The image signal in the SEM is generated serially at each point on the sample by a focused beam of electrons, while the image in the light microscope is formed by focusing light rays simultaneously from each point on the sample. Furthermore, electrons under the influence of the magnetic field of the electromagnetic lens do not travel in straight lines but are actually constrained to a spiral path through the lens (we will discuss this in greater detail later). However, the envelope of a divergent electron beam passing through a converging magnetic lens is analogous to the envelope of a divergent light beam passing through a converging glass lens; the rotary motion of the electrons does not affect the focusing properties of the lens. Hence, the simple ray diagrams for a light beam being focused through a glass lens apply equally well to the focusing of electron beams through magnetic lenses, and what we understand about cameras or light microscopy is analogous.

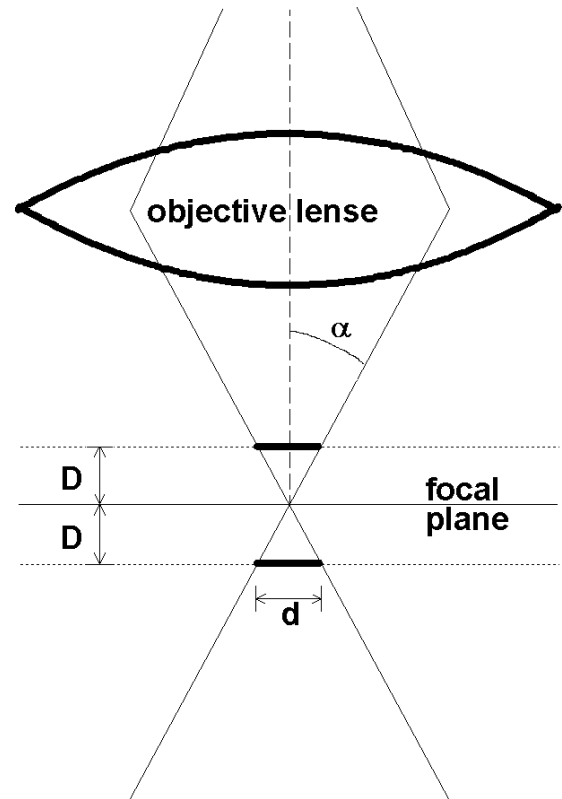


Figure 2-12 Sketch of objective lens focus illustrating the concept of *depth of field*.

In the sketch to the right,  $\alpha$  equals the half divergent angle of the objective lens. This angle is on the order of  $5 \times 10^{-3}$  radians for a typical SEM and can be as large as  $45^\circ$  (0.8 radians) for a typical high-power objective lens on a light microscope.  $D$  is the distance above and below the level (focal plane) at which a point on the specimen which is exactly in focus, and will be seen by the eye as a point. At distance  $D$  above and below, the object will be imaged as a disc of diameter  $d$  x magnification ( $M$ ).

In order for the eye to perceive the portion of the sample that is at distance  $D$  from best focus level *as if it were in focus*, the disk diameter ( $d$ ) must be less than or equal to the minimum size than can be resolved by the human eye (approximately 0.1 mm or  $10^{-4}$  m).

$$dM \leq 1 \times 10^{-4} \quad \text{but} \quad \tan \alpha = \frac{d}{2D} \quad \text{so that} \quad M2D \tan \alpha \leq 1 \times 10^{-4}$$

Therefore, the depth of field is given by:

$$2D = \frac{1 \times 10^{-4}}{M \tan \alpha}$$

eq. 2-13

Magnification	Depth of Field	
	Light Microscope ( $\alpha \gg 45^\circ$ )	SEM ( $\alpha \gg 5 \times 10^{-3}$ radians)
20X	$5 \times 10^{-6}$ m	$1000 \times 10^{-6}$ m
100X	$1 \times 10^{-6}$ m	$200 \times 10^{-6}$ m
1000X	$0.1 \times 10^{-6}$ m	$20 \times 10^{-6}$ m
10,000X		$2 \times 10^{-6}$ m
100,000X		$0.2 \times 10^{-6}$ m

### 2.6.1 Electron detectors

At this point, it might be helpful to say a few words about electron detectors as they relate to the features we have just discussed regarding SE and BSE.

The type of detector most commonly used in electron beam instruments is the *scintillator - photomultiplier system* developed into its current configuration by Everhart and Thornley in 1960. This detector, as illustrated in Figure 2-13, is based on the principle that an energetic electron striking a "scintillator" material (e.g., doped plastic, glass or a compound such as  $\text{CaF}_2$  doped with europium) produces photons. The photons produced in the scintillator are conducted through a light tube (a solid plastic or glass rod with total internal reflection) to a photomultiplier. Once the original signal is converted into light it can pass through a quartz

window into the photomultiplier which is permanently isolated from the vacuum inside the instrument. In the photomultiplier the photons strike a series of electrodes which produce a "cascade" of electrons and a measurable electrical current that is proportional to the number of photons and hence the number of secondary electrons. The output pulse of electrons can have a total gain of the order of  $10^5 - 10^6$ . This gain is produced with very little noise degradation of the original signal. Secondary electrons, with energies near 5eV, don't have sufficient energy to produce photons. To overcome this obvious problem, the scintillator is coated with a thin (10 - 50nm) film of aluminum that is positively biased to approximately +12keV. This potential accelerates the slow secondaries and imparts them with sufficient energy to produce photons within the scintillator material.

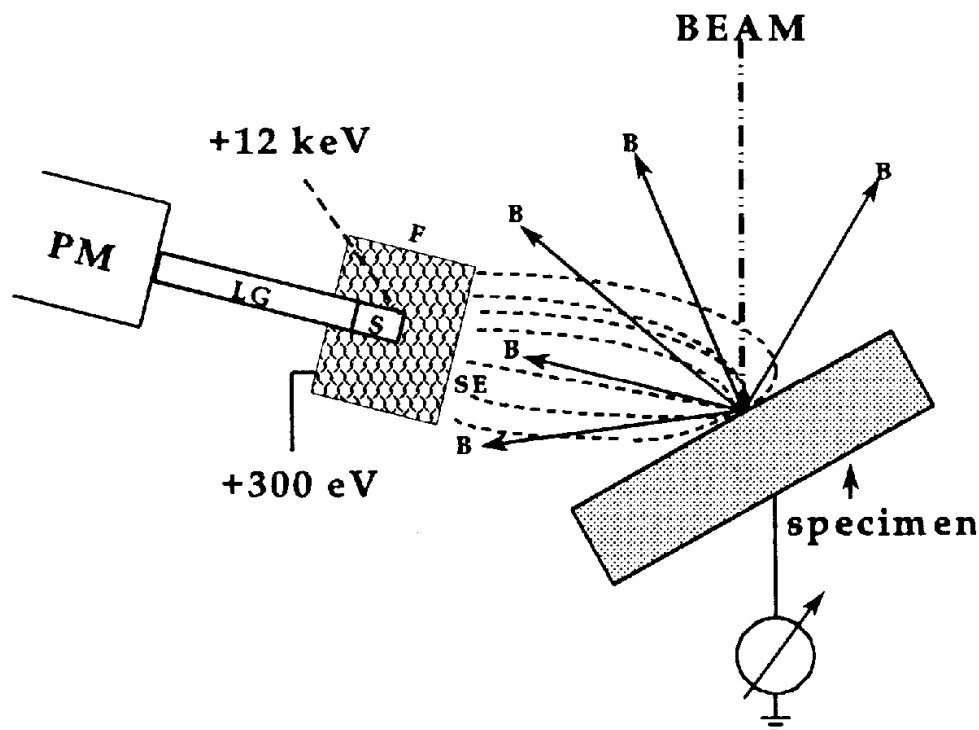


Figure 2-13 Schematic diagram of the Everhart-Thornley scintillator-photomultiplier secondary electron detector. SE, secondary electron; B, backscattered electron; F, Faraday cage; S, scintillator; LG, light guide; PM, photomultiplier.

The astute reader will question the presence and influence of a +10keV bias located in the vicinity of the electron beam. In order to prevent the 10-keV bias from deflecting the incident beam or introducing astigmatism to the beam, the biased scintillator is surrounded by a *Faraday cage* that is near ground potential (by "near ground potential" we mean at approximately 300 V). The Faraday cage effectively isolates the high positive potential to lie within the cage, and thereby shields the primary beam from the scintillator bias. In order to allow electrons to pass through the Faraday cage, it is constructed out of a wire mesh. Our new specimen-chamber camera in the JEOL SEM allows for an excellent view of the Faraday cage.

The positive bias that remains on the Faraday cage (ca. 300 V) serves an especially important role. As illustrated in Figure 2-13, this potential serves to attract the low-energy secondary electrons and pull them into the detector. Even secondary electrons with initial trajectories away from the detector are pulled back into the detector. This arrangement allows for extremely efficient collection of the low-energy secondaries.

As illustrated in Figure 2-13, backscattered electrons are also collected by the scintillator detector. Given the high energy of backscattered electrons, one might wonder how we can ever obtain a meaningful signal from the secondaries. Several factors combine to severely limit the number of BSEs that are actually collected by the SE detector. First of all, recall that the most common energy for the BSEs is typically between  $0.8$  and  $0.9E_0$  for medium- and high-atomic number materials (i.e., in the .8 to 20 keV range). Such high energy BSEs are not at all affected by the +300V "attractive force" of the Faraday cage, and hence there is no deflection of the BSEs toward the detector. BSEs therefore leave the surface of the specimen in straight line trajectories. BSEs are therefore often referred to as "line of sight" particles, meaning that only those BSEs within the line of sight toward the detector will be collected. In other words, only those BSEs with an initial trajectory directly toward the SE detector will enter the detector. Secondly, it turns out that the distribution of BSE trajectories is not uniform, but highly anisotropic.

The anisotropic nature of BSE trajectories is illustrated in Figure 2-14. In cases where the incident beam is nearly normal to the specimen, most of the BSEs have trajectories that are almost vertical. This means that in relatively flat, untilted specimens, nearly all of the BSEs will miss the SE detector if the detector is mounted at a significant angle from the vertical (as is common in all instruments). If, on the other hand, the beam strikes the specimen at a lower angle, the distribution of BSE trajectories is highly skewed in the direction away from the incident beam. With the exception of the special case in which the BSE trajectories are skewed directly toward the SE detector, this means that inclined surfaces or a tilted specimen have an insignificant number of BSEs degrading the SE signal.

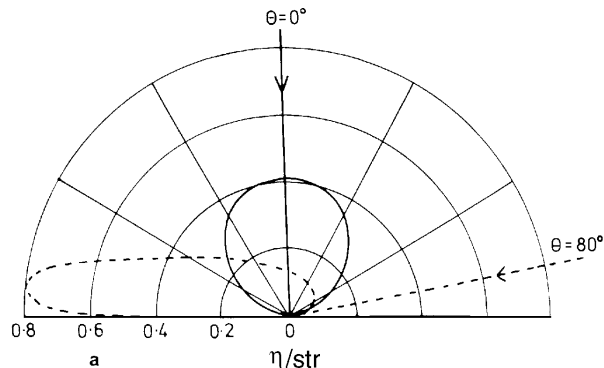


Figure 2-14 The angular distribution for backscattered electrons for beam normal to the target and for a beam highly inclined (after Goldstein, et al., 1981)

The latest generation of *backscatter* electron detectors are semi-conducting, solid-state detectors that are especially good for collecting BS electrons. Our JEOL 6300 SEM has such a detector. As noted above, for well polished, non-tilted specimens the greatest density of BSE trajectories is centered near the normal to the surface. The best place to locate a BSE detector is therefore directly above the specimen. One of the major advantages of semi-conducting, solid-state detectors is that they consist of a flat, thin (several mm) wafer that can be fabricated in a variety of shapes and sizes ... including annular detectors in the form of a ring with a hole in

the center to permit passage of the electron beam. As such, they can be located directly above the specimen at the base of the objective lens, or as it is often called, the pole piece.

A schematic explanation of a solid-state BSE detector is shown in Figure 2-15. The electronic structure of the semiconductor (in this case a silicon wafer) consists of an empty conduction band separated by a band gap from a filled valence band. When energetic BSEs enter the wafer, inelastic scattering events promote electrons from the valence band to the conduction band where they are free to move. In doing so, **electron holes** are left behind in the valence band. Left to themselves, the free electrons and the electron holes will eventually recombine. But, if an electric field is applied across the wafer, the net result is migration of valence electrons in one sense or a migration of the electron holes in the opposite sense.

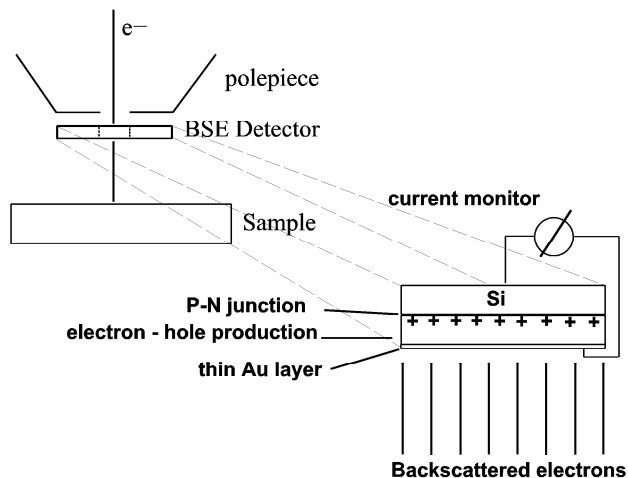


Figure 2-15 Schematic diagram of a solid state backscattered electron detector.

The latter mode of describing this type of conduction is usually adopted and the electron hole is designated as (+). The valence band electron holes in semiconductors are almost as mobile as electrons in the conduction band. When the electron holes strike a sensitive cathode they can be recorded and this event results in a signal. For Si, approximately 3.6eV is expended in creating an electron-hole pair. Thus for a single 10keV BSE entering the detector, approximately 2800 electron-hole pairs are created. This signal can then be further amplified with a current amplifier to produce a useable BSE signal for eventual CRT display.

## 2.7 Cathodoluminescence

Visible light of various wavelengths (colors) can be seen being given off from the interaction volume in a few types of materials and minerals. Some minerals will give off considerable light, e.g., benetoite (a Ba-Ti cyclo-silicate); some minerals, moderate amounts, e.g., carbonates and phosphates; in other minerals the effect is quite subtle, e.g., plagioclase. Besides being characteristic of different types of minerals, the intensity of radiation and/or its wavelengths also influenced by the presence of certain elements, e.g., rare earths; or the absence of elements, e.g., iron in plagioclase.

The CL effect has been studied most extensively in semi-conductor materials, for which the understanding is fairly straightforward, and the phenomenon can be studied in a macroscopic way. Semi-conductors have unfilled conduction bands, and unlike conductors, these bands are not readily available for valence electrons to enter; that is, there is an energy

gap to overcome and valence electrons have to be excited into these bands. If, in a semiconductor, electrons are excited into the conduction band, they will soon return if there is no potential to move them within the material, i.e. conduct. This *recombination* will give off radiation, the energy of which is relative to the energy gap, which in semi-conductors is in the range of visible light.

Since most minerals are not semi-conductors, the above explanation would seem to have little application in mineralogy. In actual fact, however, we do observe the phenomenon, and in some cases to a greater degree than in semi-conductor materials. The mechanism is not clearly understood for non-conductors, except to suppose that local regions within non-conductor lattices might exhibit semi-conductor behavior for one reason or another. Researchers of this phenomenon suspect this is so, as they have been able to correlate the presence of particle induced luminescence with lattice imperfections and impurities. The mystery remains primarily because localized defects and impurities can not be studied in a macroscopic way. The presence of elements like the lanthanides, which have in themselves electronic transitions of this magnitude, can be the sole source for this type of radiation; and in the case of certain minerals, like benitoite, the effect must be due to transition possibilities due to unique bonding characteristics.

In spite of the mystery of its origin in non-conductors, cathodoluminescence can be a useful indicator of certain types of mineralization and chemical zoning within certain minerals. For example, layers of carbonate and silica cement can be seen with much greater contrast than with light microscopy or x-rays because the luminescence is much more sensitive to subtle effects, e.g., trace elements, impurities or lattice discontinuities.

## 2.8 Summary

We have chosen to begin our study of electron probe microanalysis with specimen interaction to emphasize the source of the information we are interested in gathering. We have introduced some of the important specimen interactions before discussing the details of the hardware because we hope that an understanding of the important beam-specimen interactions will render many of the adjustable instrument parameters more relevant.

In this course we hope to expose you to most of the useful information provided by these instruments -- information from secondary electrons, backscattered electrons, cathodoluminescence, specimen current, and x-rays. There are many subtle features and artifacts involved with the generation and detection of these phenomena. By understanding them in some detail, the user is in a better position to make informed judgments regarding adjustable instrument parameters.